

Backbone NMR reveals allosteric signal transduction networks in the β_1 -adrenergic receptor

Shin Isogai¹, Xavier Deupi², Christian Opitz¹, Franziska M. Heydenreich², Ching-Ju Tsai², Florian Brueckner², Gebhard F.X. Schertler^{2,3*}, Dmitry B. Veprintsev^{2,3*} and Stephan Grzesiek^{1,*}

¹ Focal Area Structural Biology and Biophysics, Biozentrum, University of Basel, CH-4056 Basel, Switzerland

² Paul Scherrer Institute, CH-5232 Villigen PSI, Switzerland

³ Department of Biology, ETH Zurich, CH-8093 Zurich, Switzerland

***corresponding authors**

Stephan Grzesiek
Focal Area Structural Biology and Biophysics, Biozentrum
University of Basel, CH-4056 Basel, Switzerland
Phone: ++41 61 267 2100
FAX: ++41 61 267 2109
Email: Stephan.Grzesiek@unibas.ch

Dmitry B. Veprintsev
Paul Scherrer Institute, CH-5232 Villigen PSI, Switzerland
Email: dmitry.veprintsev@psi.ch

Gebhard F.X. Schertler
Paul Scherrer Institute, CH-5232 Villigen PSI, Switzerland
Email: gebhard.schertler@psi.ch

Keywords: GPCR, structure, dynamics, solution NMR, isotope labeling, chemical shift

Introduction

G protein-coupled receptors (GPCRs) are physiologically important transmembrane signaling proteins that trigger intracellular responses upon binding of extracellular ligands. Despite recent breakthroughs in GPCR crystallography¹⁻³, the details of ligand-induced signal transduction are not well understood due to missing dynamical information. In principle, such information can be provided by NMR⁴, but so far only limited data of functional relevance on few side chain sites of eukaryotic GPCRs have been obtained⁵⁻⁹. Here, we show that receptor motions can be followed at virtually any backbone site in a thermostabilized mutant of the turkey β_1 -adrenergic receptor (β_1 AR)¹⁰⁻¹². Labeling with ¹⁵N-valine in a eukaryotic expression system provides over twenty resolved resonances that report on structure and dynamics in six ligand complexes and the apo form. The response to the various ligands is heterogeneous in the vicinity of the binding pocket, but gets transformed into a homogeneous readout at the intracellular side of helix 5 (TM5), which correlates linearly with ligand efficacy for the G protein pathway. The effect of several pertinent, thermostabilizing point mutations was assessed by reverting them to the native sequence. Whereas the response to ligands remains largely unchanged, binding of the G protein mimetic nanobody NB80 and G protein activation are only observed when two conserved tyrosines (Y227 and Y343) are restored. Binding of NB80 leads to very strong spectral changes throughout the receptor including the extracellular ligand entrance pocket. This indicates that even the fully thermostabilized receptor undergoes activating motions in TM5, but the fully active state is only reached in presence of Y227 and Y343 by stabilization with a G protein-like partner. The combined analysis of chemical shift changes from the point mutations and ligand responses identifies crucial connections in the allosteric activation pathway and presents a general experimental method to delineate signal transmission networks at high resolution in GPCRs.

Results and discussion

A thermostabilized, detergent-resistant mutant of β_1 AR¹⁰⁻¹² (TS- β_1 AR; see Methods) was selectively labeled with ¹⁵N valine and produced in insect cells without further chemical modifications. Its 28 valine residues are homogeneously distributed across the receptor (Extended Data Figure 1) at locations suitable to sense ligand binding and receptor activation. Although resonances of main chain atoms are considerably more difficult to observe than those of mobile side chains of surface residues, they are expected to be better reporters of functional, long-range backbone motions. We succeeded to obtain well-resolved TROSY spectra of the valine ¹H-¹⁵N backbone resonances of detergent-solubilized TS- β_1 AR in its apo form and in complexes with six ligands (Extended Data Figure 1) ranging in their efficacy from antagonists to agonists (Extended Data Table 1). Despite the absence of deuteration and very short T₂ relaxation times (~4 ms for ¹H^N), 26 valine resonances could be observed with sufficient sensitivity and resolution. Distinct and reversible chemical shift changes were detected for many valines after ligand exchange. 16 valines were assigned unambiguously and 5 tentatively using spectra from 18 point mutants, as well as further spectral and structural information (Extended Data Table 2).

Many valine residues in the vicinity of the ligand binding pocket could be assigned, showing chemical shift changes that report on the ligand functional groups (Figure 1). Remarkably, residue V172(4.56) (the number in parenthesis corresponds to the Ballesteros-Weinstein numbering system¹³), which is located close to the ligand aromatic head group, exhibits an unusual ¹⁵N chemical shift of ~105–110 ppm (Extended Data Figure 1, 2 and Figure 1C). This anomaly seems caused by a distorted backbone geometry, which is presumably conserved among adrenergic receptors and results from a missing hydrogen bond to the proline at position 176(4.60) (Extended Data Figure 2). Instead, the carbonyl of V172(4.56) participates in a water-mediated hydrogen bond network, which connects the ligand binding site, TM3, TM4, TM5, and TM6^{12,14}. Seemingly as a result of these interactions, the V172(4.56) ¹H-¹⁵N resonances cluster according to the substitution patterns of the ligand head group (Figure 1C): one cluster is observed for the partial agonists/antagonists cyanopindolol, alprenolol and carvedilol, which have larger head groups with *ortho*- and/or *meta*-substitutions; a second cluster is observed for the agonists isoprenaline and dobutamine, which bear a *meta*- and *para*-substituted catechol ring. We attribute the distinct chemical shifts for isoprenaline or dobutamine to the loss of a coordinated water caused by specific hydrogen bond interactions between their catechol moieties and the side chain of S215(5.461) (Extended Data Figure 2D).

Remarkably, the resonance positions of V172(4.56) in complex with the antagonist atenolol strongly differ from the already described complexes and the apo form: considerable $^1\text{H}^{\text{N}}$ (>0.4 ppm) and ^{15}N (>4 ppm) upfield shifts indicate, respectively, a further weakening of the main chain hydrogen bond V172(4.56) $\text{H}^{\text{N}}\cdots\text{I168(4.52)}\text{O}$ and a stronger kink of the backbone. This rearrangement is likely due to the "insertion" of the *para*-acetamide group of the ligand head between residues S215(5.461) and V172(4.56) (Extended Data Figure 2D). This will lead to a substantial disruption of the TM3-TM4-TM5 interface, thereby precluding receptor activation, in agreement with atenolol's inverse agonist pharmacology. Thus, the amide chemical shifts of V172(4.56) constitute a very sensitive readout for the state of this water-mediated, inter-helical activation switch.

The ^1H - ^{15}N chemical shifts of further residues in the vicinity of the binding pocket report on additional characteristics of the ligands. V314(6.59) and V202(ECL2) are located at the extracellular surface of the receptor in a "vestibule" next to the entry/exit pathway of the orthosteric binding site^{15,16}. The resonances of these residues are either severely broadened or undetectable in the absence of ligands, whereas they are observable in the presence of ligands (Figure 1D and Extended Data Figure 3). A line shape analysis for V314(6.59) (Extended Data Figure 4) indicates that this extracellular part of the receptor undergoes micro- to millisecond motions in the apo form, which are quenched by ligand binding. This is consistent with results on $\beta_2\text{AR}$, which suggest that high-affinity ligands stabilize the conformation of ECL2 and ECL3⁵. The ligand-induced shifts of the V314 resonance correlate strongly ($r^2 = 0.95$) with the reported ligand affinity¹⁷ (Figure 1D). Interestingly, the resonances of V314(6.59) in the apo form and in high-affinity ligand complexes are very close. This may indicate that the high-affinity ligand complexes mimic the average apo conformation. Finally, the ^1H - ^{15}N chemical shifts of V125(3.36) at the bottom of the binding site and of V103(2.65) close to the ligand tail reveal additional trends (Figure 1E): the chemical shifts of V125 correlate with the depth of ligand insertion towards the central part of TM3 ($r^2 = 0.81$), whereas those of V103 correlate with the volume of the ligand tail ($r^2 = 0.90$).

As compared to inactive $\beta_2\text{AR}$, complexes of activated $\beta_2\text{AR}$ with either G protein² or the G protein-mimicking nanobody NB80^{9,18} show large movements at the intracellular sides of TM5, TM6 and their intervening loop ICL3, which form the binding site for the G protein. These conformational changes are expected to be conserved throughout the GPCR family¹⁹. Four valine residues could be assigned in this region of TS- $\beta_1\text{AR}$: V226(5.57), V230(5.61), V280(6.25), and V298(6.43) (Figure 2). In contrast to the chemical shift changes in the

vicinity of the ligand binding pocket, which depend strongly on the ligand chemistry, the shifts of the TM5 residues observed in this region report on ligand efficacy. This effect is most prominent for residue V226(5.57), for which the ^1H - ^{15}N resonances fall on one line from antagonists to agonists (Figure 2A). The chemical shifts for the different ligands correlate very strongly ($r^2 = 0.89$) with their reported¹⁷ efficacies for Gs signaling (Extended Data Table 1). This highly linear effect suggests that the receptor filters the diverse input signals from the various ligands to a unified and precise structural response on TM5, which can be read out by the chemical shifts of V226(5.57). Interestingly, the V226(5.57) atenolol peak is situated at a position corresponding to lower efficacy than for the apo receptor. This gives direct structural evidence of atenolol's inverse agonist action, which reduces the activation relative to the basal level of the apo receptor.

Current high-resolution structures of $\beta_1\text{AR}$ do not show significant changes between antagonist- and agonist-bound forms (Figure 2B, top panel). The decrease of the V226(5.57) $^1\text{H}^{\text{N}}$ chemical shift by about 0.2 ppm from the agonist isoprenaline to the antagonist atenolol indicates a lengthening of the V226(5.57)- $\text{H}^{\text{N}}\cdots\text{I222(5.53)}\text{-O}$ hydrogen bond by about 0.05 Å²⁰. This small, but clearly NMR-detectable length variation is below the resolution limit of current GPCR structures (Supplementary Information Text 1), but may indicate the start of TM5 bending towards the active conformation as observed in the G protein-bound form of $\beta_2\text{AR}$ (Figure 2B). Remarkably, this response to agonists occurs even in the thermostabilized receptor TS- $\beta_1\text{AR}$. Albeit reduced in absolute size as compared to V226(5.57), V230(5.61) displays similar linear chemical shift changes as a function of ligand efficacy for the Gs pathway (Figure 2C). As this residue is located one helical turn further towards the cytoplasm, the detected conformational change is not just local, but spans a certain length in TM5.

Compared to V226(5.57) and V230(5.61) in TM5, the chemical shift response to ligands is much less pronounced for V298(6.43) and in particular V280(6.25) at the intracellular side of TM6 (Figure 2C). This suggests that agonist binding to the TS- $\beta_1\text{AR}$ does not induce the large conformational change in TM6 observed in the activated $\beta_2\text{AR}$ -G-protein² or $\beta_2\text{AR}$ -NB80¹⁸ complexes. However, G protein activation upon agonist binding has been reported for other less thermostabilized $\beta_1\text{AR}$ constructs¹⁷, indicating that they can still be activated, albeit at low levels. Thus we reverted the mutations most likely to interfere with the activation mechanism in TS- $\beta_1\text{AR}$, i.e. I129(3.40)V in the connector switch¹⁵, Y227(5.58)A in TM5^{21,22}, and Y343(7.53)L in the NPxxY motif of TM7^{14,22} to the native residues. These reverse mutants were then tested for G protein activation and the NMR response in TM6. A summary of the

results is given in Extended Data Table 3. The original TS- β_1 AR, the single mutants TS- β_1 AR_{V129I}, TS- β_1 AR_{A227Y}, and TS- β_1 AR_{L343Y} as well as the double mutant TS- β_1 AR_{V129I/A227Y} showed no detectable G protein activation upon isoprenaline binding (Extended Data Figure 5). However, G protein activation was detectable for the least thermostable TS- β_1 AR_{A227Y/L343Y} double mutant (T_m reduced by 11 °C relative to TS- β_1 AR), which recovers the conserved tyrosines in TM5 and TM7 that are known to stabilize the active state of rhodopsin²². None of the reverse mutants showed major changes in the NMR spectra of various ligand complexes as compared to the original TS- β_1 AR (Extended Data Figure 6). In particular, residues V298(6.43) and V280(6.25) at the intracellular side of TM6 did not show an increased response to agonists. This is in agreement with recent DEER and ¹⁹F-NMR data showing that agonists alone do not fully stabilize the active state of TM6 in β_2 AR⁹. Interestingly, the V129(3.40)I and the V129(3.40)I/A227(5.58)Y mutations shifted the ¹H-¹⁵N resonances of V226(5.57) towards a more active (i.e. bent) state of TM5 in both the atenolol- and isoprenaline-bound forms (Extended Data Figure 6B), thereby given direct experimental evidence for an allosteric activation pathway spanning about 13 Å from I129(3.40) on TM3 to V226(5.57) on TM5.

With the exception of rhodopsin²³, the stabilization of fully active GPCR conformations seems to require binding of an agonist and an intracellular partner^{8,9}. Indeed, when both the agonist isoprenaline and the G protein-mimicking nanobody NB80¹⁸ were added to TS- β_1 AR_{A227Y/L343Y}, very large chemical shift responses for many valine residues in TM3-6 were observed, whereas no change was observed for several valines in TM1, 2, and 7 (Extended Data Figure 7). This very strong response extends even to the extracellular residue V314(6.59), providing evidence of a long-distance connection from the G protein binding site to the ligand entry site. The strong chemical shift changes are reverted when the partial agonist/antagonist cyanopindolol is added to the isoprenaline-TS- β_1 AR_{A227Y/L343Y}-NB80 complex. The spectrum then becomes identical to that of the “pure” cyanopindolol-TS- β_1 AR_{A227Y/L343Y} complex (Extended Data Figure 7A), indicating that cyanopindolol replaces isoprenaline and causes the release of NB80. In agreement with the G protein activation data, the isoprenaline-bound original TS- β_1 AR and the mutants TS- β_1 AR_{A227Y} and TS- β_1 AR_{L343Y} did not show binding of NB80 in the NMR spectra. Moreover, supplementing NB80 to the ultrastable TS- β_1 AR did not change its affinity for isoprenaline (Extended Data Figure 7B), whereas it caused a hundred-fold affinity increase for TS- β_1 AR_{A227Y/L343Y} and the truncated

native turkey β_1 AR receptor (t β trunc)¹⁷. This increase is identical to data for β_2 AR¹⁸ and shows the energetic coupling between the NB80 and agonist binding also for β_1 AR.

In combination, these data prove that agonist binding, even in the absence of a G protein-mimic, induces or stabilizes initial changes in the conformational equilibrium of TM5 towards the conformation observed in the G protein complex of β_2 AR. Remarkably, these rearrangements occur in all thermostabilized forms of β_1 AR. However, a full shift of the equilibrium towards such an active conformation including allosteric changes at the extracellular side occurs only when G protein or its mimetic NB80 is bound. This process requires the presence of both Y227(5.58) and Y343(7.53), which significantly reduce the thermal stability. Different active conformations may be reached for non-G protein effectors such as β -arrestin.

The possibility to detect NMR signals at many receptor sites in response to ligand binding and point mutations provides an experimental method to trace allosteric signaling paths. Figure 3 shows examples of these pathways, derived from the response to the ligands atenolol and isoprenaline and the single point mutations V129(3.40)I, A227(5.58)Y, and L343(7.53)Y. Choosing a cutoff of 0.05 ppm for the resulting combined ¹H, ¹⁵N chemical shift change (Figure 3A, red line), long-range (>10 Å) connections become evident throughout the receptor (Figure 3B and C). Whereas detected ligand signals radiate broadly to almost all helices, the point mutants give evidence of smaller interaction networks connecting TM3 to TM4/5, TM5 to TM3/4/6, as well as TM7 to TM2/3 (Figure 3B,C). Interestingly, the TM2/TM7 network appears to be only weakly connected to the TM3-6 network. Together, these data provide experimental evidence at high resolution of an extensive signal transduction network that connects the ligand binding site to the intracellular sides of TM5, TM6, and TM7. Such a network of loosely coupled allosteric connections has been postulated previously for β_2 AR based on molecular dynamics simulations²⁴.

In summary, we have shown that highly resolved solution NMR backbone spectra can be obtained for a eukaryotic GPCR. The NMR observations delineate the allosteric signaling pathways and comprehensively connect many previous experimental and theoretical observations, which may ultimately allow to understand the dynamic mechanisms of GPCRs at the atomic level.

Acknowledgments

We gratefully acknowledge Dr. Timothy Sharpe of the Biozentrum Biophysics Facility for expert help with biophysical assays. We thank Prof. Jan Steyaert (Vrije Universiteit Brussel) for providing the NB80 plasmid and Marco Rogowski for preparing wild-type β_1 AR baculovirus. FB was supported by Marie Curie and EMBO postdoctoral fellowships. This work was supported by Swiss National Science Foundation grants 31-132857 (S.G.), Sinergia 141898 (SG, DBV, GFXS), 31-135754 (DBV), 31-153145 (GFXS), 31-146520 (XD), and COST Action CM1207 (GLISTEN) (XD and GFXS).

Author Contributions

S.G., G.F.X.S., D.B.V., X.D. and S.I. initiated and managed the project. S.I., X.D., F.B., D.B.V., G.F.X.S. and S.G. designed ligand response and selective labeling experiments. C.O. designed initial TS- β_1 AR construct and established purification. S.I. designed and prepared all selectively labeled receptor mutants, performed ligand exchange, NB80 binding, and all NMR experiments. S.I. and S.G. designed NMR experiments, analyzed and interpreted all data. F.M.H. and D.B.V. purified trimeric G_i protein, designed and performed radioligand affinity and G_i protein activation assays. C.J.T. prepared NB80 nanobody. S.G., S.I., X.D., F.M.H., D.B.V. and G.F.X.S. wrote the manuscript.

Author Information

The authors declare no competing financial interests.

Methods

β_1 AR constructs

The TS- β_1 AR mutant was derived from the turkey β_1 AR44-m23 mutant used in crystallographic studies²⁵ by adding three additional thermostabilizing mutations (I129V, D322K, and Y343L) and a neutral mutation (D200E) from the ultra-stable β_1 AR-JM3 mutant¹¹. As compared to the wild type, TS- β_1 AR contains truncations at the N- and C-termini and intracellular loop (ICL3), a total of nine thermostabilizing point mutations, three further point mutations as well as a C-terminal hexahistidine tag (Extended Data Figure 1). The final TS- β_1 AR sequence is

```
MGAELLSQQWEAGMSLLMAL  VVLLIVAGNVLVIAAIGSTQ  RLQTLTNLFITSLACADLVV
GLLVVPPFGATLVVRGTWLWG  SFLCELWTSLDVLCVTASVE  TLCVIAIDRYLAITSPFRYQ
SLMTRARAKVICTVWAISA    LVSFLPIMMHWRDEDPQAL   KCYQDPGCEFFVTNRAYAIA
SSIISFYIPLLIMIFVALRV   YREAKEQIRKIDRASKRKTS  RVMLMREHKALKTLGIIMGV
FTLCWLPFFLVNIVNVFNRD   LVPKWLFFVAFNWLGYANSAM NPIILCRSPDFRKAFFKRLLA
FPRKADRRLHHHHHH.
```

Additional valine-to-alanine or isoleucine point mutations were introduced into TS- β_1 AR for NMR assignment purposes. All constructs were made using the QuikChange site-directed mutagenesis method (Agilent). Baculovirus for insect cell expression was generated using the Bac-to-Bac system (Invitrogen).

β_1 AR expression and purification

All β_1 AR constructs were expressed in baculovirus-infected insect cells as described²⁶. Selective labeling by ¹⁵N-valine was achieved by growing cells on unlabeled serum-free insect cell medium (InsectXpress, Lonza) and then exchanging into custom-made serum-free medium (SF4, BioConcept) devoid of valine and yeast extract, to which 100 mg/L ¹⁵N-valine were supplemented. Virus was added immediately after the medium exchange. The culture was harvested at 48 or 72 hr post infection.

After cell lysis, the membrane fraction was separated from the lysate via ultracentrifugation and subsequently solubilized with 2 % *n*-decyl- β -D-maltopyranoside (DM, Anatrace). The solubilized membrane fraction was then purified by nickel ion affinity chromatography followed by alprenolol ligand affinity chromatography. The active receptor was eluted with buffer (20 mM TRIS, 350 mM NaCl, 0.1 % DM, pH 7.5) containing either atenolol (1 mM) or alprenolol (0.1 mM). Final yields of detergent-solubilized receptor were

1.5 mg/L of cell culture. The molecular weight of the receptor-detergent complex was estimated as ~100 kDa by static light scattering.

Thermal shift assays of mutant receptors

Detergent-solubilized, purified apo TS- β_1 AR and reverse-mutation receptors for thermal stability assays were obtained from their atenolol-bound form by washing with buffer devoid of ligand on a HiTrap SP HP (GE Healthcare) column. Their thermal stability was determined by the microscale fluorescent stability assay for binding of the thiol-specific fluorochrome N-[4-(7-diethylamino-4-methyl-3-coumarinyl)phenyl]maleimide (CPM)²⁷ in a Rotor-Gene Q (QIAGEN) real-time PCR cycler using 1 μ g of receptor in 20 mM TRIS, 350 mM NaCl, 0.1 % DM, pH 7.5 and a heating rate of 2 K/min.

NMR experiments

NMR samples were prepared in Shigemi tubes as 250 μ l volumes of typically 100 μ M receptor, 1 mM ligand (except for apo form), 20 mM TRIS, 100 mM NaCl, 0.1 % DM, 5 % D₂O, pH 7.5. For isoprenaline or dobutamine, 2 mM of sodium L-ascorbate were supplemented as anti-oxidant. All solution NMR measurements were carried out on a 800 MHz or a 900 MHz Bruker Avance III spectrometer equipped with a cryogenic probe at 304 K. 2D ¹H,¹⁵N TROSY (transverse relaxation-optimized spectroscopy) spectra were recorded with total acquisition periods of 16 ms (¹⁵N) and 43 ms (¹H) with typical total experimental times of 24-48 h. As compared to a standard TROSY pulse sequence, the ¹H-¹⁵N INEPT delays were set to 3 ms to reduce magnetization losses from relaxation.

Assignment procedure

To obtain sequence-specific assignment information, we initially attempted to detect HNCO and HNCA correlations on samples additionally labeled with ¹³C at specific backbone sites²⁸. However, due to low sensitivity, only very few correlations were observable. Therefore, assignments were obtained from a combination of information from TROSY spectra recorded on 18 TS- β_1 AR valine point mutants with different ligands, four HN(CO) correlations and five distinct structure-based chemical shift predictions (Extended Data Table 2).

Ligand exchange experiments

Receptor complexes with different ligands were generated by sequential exchange according to increasing ligand affinity, i.e. in the sequence atenolol-isoprenaline-dobutamine-alprenolol or alprenolol-carvedilol-cyanopindolol. For exchange, the sample was washed three times with buffer devoid of ligand at 10-fold dilution in Amicon Ultra 50 kDa cutoff

concentrators. Subsequently, the sample was washed again twice with buffer containing 100 μM new ligand, separated by a period of 1 h incubation. Final concentrations of the ligands were adjusted to 1 mM. Apo receptor was generated from the atenolol complex by six washing steps of 10-fold dilution in ligand-free buffer using a 1 h incubation period for the last three steps.

NMR NB80 binding experiment

Binding of NB80 to $\beta_1\text{AR}$ mutants was assessed using TROSY and 1D proton NMR spectra. These spectra were recorded on the $\beta_1\text{AR}$ mutants (TS- $\beta_1\text{AR}$: 132 μM , TS- $\beta_1\text{AR}_{\text{A227Y}}$: 120 μM , TS- $\beta_1\text{AR}_{\text{L343Y}}$: 110 μM , and TS- $\beta_1\text{AR}_{\text{A227Y/L343Y}}$: 120 μM) in the presence of saturating amounts (1 mM) of the agonist isoprenaline before and immediately after addition of an equimolar (relative to the receptor) amount of NB80. For TS- $\beta_1\text{AR}_{\text{A227Y/L343Y}}$ additional spectra were recorded after a further addition of the partial agonist cyanopindolol (1 mM) to the already present isoprenaline and NB80.

Scintillation proximity assay with ^3H -dihydroalprenolol

For pharmacological binding assays membranes were prepared from SF9 insect cells as described previously²⁶. The total protein content of the membranes was estimated by A280 measurements using an average extinction coefficient of 1.0 per mg/ml. All assays were carried out in 96-well plates at 200 $\mu\text{g/ml}$ total protein in membranes and 2 mg/ml WGA-YSi beads (Perkin-Elmer) in a 100 μl total volume per well. Samples were equilibrated at room temperature for at least 16 h. K_D values for the radioactive ligand ^3H -dihydroalprenolol (^3H -DHA) were determined by titrating ^3H -DHA from 0.032 to 100 nM. Non-specific binding was determined in presence of 1 μM S-propranolol to block the ligand binding site. Competition assays were performed in the presence of 20 nM ^3H -DHA (hot ligand) and increasing concentrations of the competitor (cold ligand). Dilutions of alprenolol, atenolol, cyanopindolol, dobutamine and isoprenaline were made with phosphate buffered saline (PBS, Biochrom, Germany). Due to the limited solubility of carvedilol in water, stock dilutions of carvedilol were prepared in DMSO. The final concentration of DMSO in the samples was 5 %. To test the effect of NB80 binding on the affinities (IC_{50}) of isoprenaline for various receptor mutants, the competition assays were also carried out in the presence of saturating concentrations of NB80 (10 μM). IC_{50} values were determined by fitting the measured radioactive counts per minute $CPM(X)$ at a specific concentration X of the competitor to the equation $CPM(X) = \frac{CPM_{max} - CPM_{min}}{1 + \frac{X}{IC_{50}}} + CPM_{min}$, where CPM_{max} and CPM_{min} are maximal and minimal counts of the assay, respectively. The fits were carried in MATLAB

(MathWorks, www.mathworks.com) with Monte-Carlo estimation of errors. K_i values were calculated from the obtained IC_{50} values according to the formula $K_i = \frac{IC_{50}}{1 + \frac{A}{K_D}}$ where A is the concentration of the radioactive ligand and K_d is its affinity for the receptor determined in the direct binding experiment.

G protein activation assay

G protein activation was measured on purified β_1 AR mutants reconstituted with MSP1E3D1²⁹ into POPC/POPG nanodiscs. MSP1E3D1 was expressed and purified as described²⁹ and cleaved with TEV protease. 1-palmitoyl-2-oleoyl-*sn*-glycero-3-phosphocholine (POPC, Avanti Polar Lipids) and 1-palmitoyl-2-oleoyl-*sn*-glycerol-3-phospho-(1'-*rac*-glycerol) sodium salt (POPG, Avanti Polar Lipids) were solubilized at a ratio of 1:1.5 (w/w) POPG/POPC in ND buffer (20 mM HEPES pH 8, 100 mM NaCl, 1 mM EDTA) with 50 mM sodium cholate (Sigma-Aldrich) at 4 °C. 133.3 μ M MSP1E3D1 was incubated with 8 mM solubilized POPC/POPG and 10 μ M purified β_1 AR in ND buffer with a final concentration of 24 mM sodium cholate for 1 h at 4 °C. Nanodiscs containing the receptor were separated from empty nanodiscs using a cobalt-chelating resin. The heterotrimeric G protein was prepared by incubating 10 μ M recombinant G α i1 and 10 μ M native G β \gammat in activation buffer (25 mM HEPES pH 7.5, 150 mM NaCl, 2 mM MgCl₂, 1 mM DTT) for 30 min at 4 °C.

G protein activation was detected by the change in tryptophan fluorescence caused by the exchange of GDP for GTP γ S, associated conformational changes in the G α subunit and its dissociation from the G β \gamma subunit of the heterotrimeric G protein³⁰. All measurements were carried out on a Varian Cary Eclipse fluorescence spectrophotometer (λ_{ex} = 295 nm, λ_{em} = 340 nm, 1.5 nm excitation slit, 20 nm emission slit, 2 s averaging time, 15 s cycle time) using final sample volumes of 1 ml in 10x4 mm cuvettes (Hellma, CH) and magnetic stirrers at 20 °C. Prior to activation, the fluorescence intensity baseline was recorded with 100 nM heterotrimeric G protein for approximately 500 s. The activation was started by adding 6 nM β_1 AR and 10 μ M GTP γ S, and the fluorescence intensity was monitored for a further 1 h. For experiments in the presence of an agonist, the concentrated receptor stock solution (1.5 μ M) was pre-incubated for 30 min at 4 °C with 40 μ M isoprenaline, and the buffer during the measurements contained 2 μ M of isoprenaline to maintain the saturation conditions for the receptor.

Figure legends

Figure 1: Ligand-induced ^1H - ^{15}N chemical shift changes in the vicinity of the ligand binding pocket of $\beta_1\text{AR}$.

(a) Partial view of the $\beta_1\text{AR}$ -carvedilol crystal structure (4AMJ) showing valine residues (blue spheres) in the vicinity ($< 8.5 \text{ \AA}$) of the ligand (magenta sticks) binding site.

(b) Chemical structures of the $\beta_1\text{AR}$ ligands used in this study. Ligand affinities derived from whole cell binding assays on the thermostabilized $\beta_36\text{-m}23 \beta_1\text{AR}$ construct¹⁷ are indicated as pK_D values. Similar pK values were measured for the TS- $\beta_1\text{AR}$ construct (Extended Data Table 1).

(c, left) Ligand-induced response of V172(4.56) ^1H - ^{15}N resonances. The black bar represents a scale of 0.1 ppm (^1H) and 1 ppm (^{15}N). The labels *o*, *m*, *p* indicate respectively ligands with *ortho*, *meta*, and *para* substitutions at the head group.

(c, right) Partial view of the $\beta_1\text{AR}$ -carvedilol structure (4AMJ) showing the interaction network connecting V172(4.56) to S215(5.461), P219(5.50), I129(3.40), and F299(6.44).

(d, left) Representation as (c, left) for the ^1H - ^{15}N resonances of V314(6.59). Centers of resonances are indicated by circles.

(d, middle) Correlation of a best-fit linear combination of the V314(6.59) chemical shifts ($48.9 \delta^1\text{H} + 0.986 \delta^{15}\text{N} - 488$) to the ligand affinity pK_D (Extended Data Table 1).

(d, right) Partial view of the carvedilol (red, 4AMJ), dobutamine (orange, 2Y01), cyanopindolol (green, 2VT4 B), and isoprenaline (blue, 2Y03) complex structures showing the ligand-induced movement of V314(6.59).

(e, left) Representation as (d, left) for the ^1H - ^{15}N resonances of V125(3.36) and V103(2.65).

(e, middle) Correlations of best-fit linear combinations of chemical shifts for V125(3.36) ($-0.402 \delta^1\text{H} + 1.17 \delta^{15}\text{N} - 132$) and V103(2.65) ($-336 \delta^1\text{H} - 634 \delta^{15}\text{N} + 7.64 \cdot 10^4$) to the ligand insertion depths and tail volumes (Extended Data Table 1), respectively.

(e, right) Partial view of the carvedilol, dobutamine, cyanopindolol, and isoprenaline crystal structures (representation as d, right) showing the ligand-induced movement of V125(3.36), D121(3.32), and V103(2.65).

Figure 2: Correlation of ligand-induced chemical shift changes at the TS- $\beta_1\text{AR}$ intracellular side with Gs efficacy.

(a, top) Response of the V226(5.57) ^1H - ^{15}N resonance to various ligands (color coding as in Figure 1). The centers of resonances are indicated by circles. The ^1H - ^{15}N resonances fall on one line from atenolol (antagonist) over apo to alprenolol (partial agonist), carvedilol (antagonist), cyanopindolol (partial agonist), dobutamine (full agonist) and isoprenaline (full agonist).

(a, bottom) Correlation of a best-fit linear combination of the V226(5.57) chemical shifts ($-515 \delta^1\text{H} - 31.7 \delta^{15}\text{N} + 8.41 \cdot 10^3$) in different ligand complexes to their efficacy for the Gs signaling pathway¹⁷.

(b, top) Overlay of TM5 and TM6 backbones of thermostabilized $\beta_1\text{AR}$ in antagonist- (blue, PDB code 4AMJ) and agonist-bound (green, PDB code 2Y03) form. The agonist does not induce detectable helix movements.

(b, bottom) TM5 and TM6 backbone movements upon activation in human $\beta_2\text{AR}$. The overlay of inactive (blue, PDB code 2RH1) and G protein-bound $\beta_2\text{AR}$ (magenta, PDB code 3SN6)

structures shows the large bend of TM6 along with the smaller conformational change of TM5 upon activation. Hydrogen bonds 5.57-H^N...5.53-O and 5.61-H^N...5.57-O are indicated by dashes. According to the behavior of the ¹H^N chemical shifts of V226(5.57) and V230(5.61) in TS-β₁AR, these hydrogen bonds expand in an efficacy-dependent manner during agonist binding.

(c) Response of the ¹H-¹⁵N resonances for V226(5.57), V230(5.61), V298(6.43), and V280(6.25) to various ligands. For clarity, only the centers of resonances are depicted as circles with color coding as in Figure 1. The black bar represents a scale of 0.1 ppm and 1 ppm for the ¹H and ¹⁵N chemical shifts, respectively. The schematic representation of the receptor indicates the locations of the respective valine residues at the cytoplasmic sides of TM5 and TM6 within the helical bundle of β₁AR.

Figure 3: Experimental detection of allosteric signaling pathways using the NMR response to ligand binding and point mutations at different backbone sites.

(a) Combined ¹H, ¹⁵N chemical shift deviations [$\Delta\delta = (\Delta\delta_{\text{1H}}^2/2 + \Delta\delta_{\text{15N}}^2/50)^{1/2}$] of valine resonances observed upon ligand binding or induced by the indicated point mutations. For ligand binding, the three pairwise deviations $\Delta\delta$ were calculated between the apo, atenolol-, and isoprenaline-bound forms of TS-β₁AR. The maximum of these deviations is shown. For the reverse mutants, deviations $\Delta\delta$ are shown relative to TS-β₁AR for their apo (black), atenolol- (cyan), and isoprenaline-bound (blue) bound forms. Valines within 10 Å from the C^α atom of the mutated amino acid are shown on a grey background. Distances were calculated using the coordinates of the thermostabilized β₁AR (PDB code 4BVN). A red line marks a cut-off value $\Delta\delta$ of 0.05 ppm for significant chemical shift deviations.

(b) Topology of the signaling network determined from point mutations (left) and ligand binding (right). Signal paths were identified by chemical shift deviations $\Delta\delta$ larger than 0.05 ppm induced by these two perturbations (panel a). Signal paths to valines within 10 Å from the ligand or point mutation (i.e. localized conformational changes) are indicated as dashed lines, and those beyond 10 Å (long-range conformational changes) as solid lines. The ligand signals broadly towards all helices but TM1. In contrast, the network determined by the point mutations is more localized and connects TM3 to TM4/5, TM5 to TM3/4/6, and TM7 to TM2/3. The latter network appears to be divided into two subnetworks involving TM3/4/5/6 and TM2/7.

(c) Long-range allosteric signal paths identified from ligand binding or point mutations (Figure 3a and b) indicated on schematic β₁AR representations showing the involved TMs. Helices are color-coded according to panel b.

References

1. Rasmussen, S. G. F. *et al.* Crystal structure of the human beta2 adrenergic G-protein-coupled receptor. *Nature* **450**, 383–387 (2007).
2. Rasmussen, S. G. F. *et al.* Crystal structure of the b2 adrenergic receptor–Gs protein complex. *Nature* **477**, 549–555 (2011).
3. Ghosh, E., Kumari, P., Jaiman, D. & Shukla, A. K. Methodological advances: the unsung heroes of the GPCR structural revolution. *Nat Rev Mol Cell Biol* **16**, 69–81 (2015).
4. Grzesiek, S. & Sass, H.-J. From biomolecular structure to functional understanding: new NMR developments narrow the gap. *Curr. Opin. Struct. Biol.* **19**, 585–595 (2009).
5. Bokoch, M. P. *et al.* Ligand-specific regulation of the extracellular surface of a G-protein-coupled receptor. *Nature* **463**, 108–112 (2010).
6. Kofuku, Y. *et al.* Efficacy of the β 2-adrenergic receptor is determined by conformational equilibrium in the transmembrane region. *Nat Commun* **3**, 1045–9 (2012).
7. Liu, J. J., Horst, R., Katritch, V., Stevens, R. C. & Wuthrich, K. Biased Signaling Pathways in β 2-Adrenergic Receptor Characterized by 19F-NMR. *Science* **335**, 1106–1110 (2012).
8. Nygaard, R. *et al.* The dynamic process of β (2)-adrenergic receptor activation. *Cell* **152**, 532–542 (2013).
9. Manglik, A. *et al.* Structural Insights into the Dynamic Process of β 2-Adrenergic Receptor Signaling. *Cell* **161**, 1101–1111 (2015).
10. Warne, T. *et al.* Structure of a beta1-adrenergic G-protein-coupled receptor. *Nature* **454**, 486–491 (2008).
11. Miller, J. L. & Tate, C. G. Engineering an ultra-thermostable β (1)-adrenoceptor. *J. Mol. Biol.* **413**, 628–638 (2011).
12. Miller-Gallacher, J. L. *et al.* The 2.1 Å Resolution Structure of Cyanopindolol-Bound β 1-Adrenoceptor Identifies an Intramembrane Na⁺ Ion that Stabilises the Ligand-Free Receptor. *PLoS ONE* **9**, e92727 (2014).
13. Ballesteros, J. A. & Weinstein, H. Integrated methods for the construction of three-dimensional models and computational probing of structure-function relations in G protein-coupled receptors. *Methods in Neurosciences* **25**, 366–428 (1995).
14. Deupi, X. & Standfuss, J. Structural insights into agonist-induced activation of G-protein-coupled receptors. *Curr. Opin. Struct. Biol.* **21**, 541–551 (2011).
15. Dror, R. O. *et al.* Pathway and mechanism of drug binding to G-protein-coupled receptors. *Proc. Natl. Acad. Sci. USA* **108**, 13118–13123 (2011).
16. Gonzalez, A., Perez-Acle, T., Pardo, L. & Deupi, X. Molecular basis of ligand dissociation in β -adrenergic receptors. *PLoS ONE* **6**, e23815 (2011).
17. Baker, J. G., Proudman, R. G. W. & Tate, C. G. The pharmacological effects of the thermostabilising (m23) mutations and intra and extracellular (β 36) deletions essential for crystallisation of the turkey β -adrenoceptor. *Naunyn Schmiedebergs Arch. Pharmacol.* **384**, 71–91 (2011).
18. Rasmussen, S. G. F. *et al.* Structure of a nanobody-stabilized active state of the β (2) adrenoceptor. *Nature* **469**, 175–180 (2011).
19. Manglik, A. & Kobilka, B. The role of protein dynamics in GPCR function: insights from the β 2AR and rhodopsin. *Curr. Opin. Cell Biol.* **27**, 136–143 (2014).
20. Grzesiek, S., Cordier, F., Jaravine, V. & Barfield, M. Insights into biomolecular hydrogen bonds from hydrogen bond scalar couplings. *Prog Nucl Mag Res Sp* **45**, 275–300 (2004).
21. Tate, C. G. & Schertler, G. F. Engineering G protein-coupled receptors to facilitate their structure determination. *Curr. Opin. Struct. Biol.* **19**, 386–395 (2009).

22. Goncalves, J. A. *et al.* Highly conserved tyrosine stabilizes the active state of rhodopsin. *Proc. Natl. Acad. Sci. USA* **107**, 19861–19866 (2010).
23. Park, J. H., Scheerer, P., Hofmann, K. P., Choe, H.-W. & Ernst, O. P. Crystal structure of the ligand-free G-protein-coupled receptor opsin. *Nature* **454**, 183–187 (2008).
24. Dror, R. O. *et al.* Activation mechanism of the β 2-adrenergic receptor. *Proc. Natl. Acad. Sci. USA* **108**, 18684–18689 (2011).
25. Warne, T. *et al.* The structural basis for agonist and partial agonist action on a β 1-adrenergic receptor. *Nature* **469**, 241–244 (2011).
26. Brueckner, F. *et al.* Structure of β -adrenergic receptors. *Meth Enzymol* **520**, 117–151 (2013).
27. Alexandrov, A. I., Mileni, M., Chien, E. Y. T., Hanson, M. A. & Stevens, R. C. Microscale fluorescent thermal stability assay for membrane proteins. *Structure* **16**, 351–359 (2008).
28. Vajpai, N. *et al.* Backbone NMR resonance assignment of the Abelson kinase domain in complex with imatinib. *Biomol NMR Assign* **2**, 41–42 (2008).
29. Bayburt, T. H., Grinkova, Y. V. & Sligar, S. G. Self-Assembly of Discoidal Phospholipid Bilayer Nanoparticles with Membrane Scaffold Proteins. *Nano Lett.* **2**, 853–856 (2002).
30. Ernst, O. P., Bieri, C., Vogel, H. & Hofmann, K. P. Intrinsic biophysical monitors of transducin activation: fluorescence, UV-visible spectroscopy, light scattering, and evanescent field techniques. *Meth Enzymol* **315**, 471–489 (2000).
31. Han, B., Liu, Y., Ginzinger, S. W. & Wishart, D. S. SHIFTX2: significantly improved protein chemical shift prediction. *J. Biomol. NMR* **50**, 43–57 (2011).

Extended Data figure and table legends

Extended Data Figure 1: Position of valine residues in the thermostabilized mutant TS- β_1 AR.

(a) Schematic representation of secondary structure and amino acid sequence of TS- β_1 AR. As compared to the wild type, the TS- β_1 AR has truncations at the N- and C-termini and the intracellular loop (ICL3) as well as nine thermostabilizing point mutations (color coded green) and three additional point mutations (color coded yellow). Valines labeled with ^{15}N are indicated by bold circles for assigned (blue) and unassigned (grey) residues.

(b) Structure of β_1 AR in complex with carvedilol (PDB code 4AMJ). The protein backbone and carvedilol are shown in ribbon and red stick representation, respectively. The individual valines are depicted as spheres (blue: assigned, grey: not assigned) labeled by residue number.

(c) Full ^1H - ^{15}N TROSY spectra of apo TS- β_1 AR and all investigated ligand complexes. The ligand chemical structures are shown as inserts. Resonances are marked with assignment information (black: firm, cyan: tentative).

Extended Data Figure 2: Effect of ligand head group substitution on hydrogen bond network involving V172(4.56) in β_1 AR.

(a) Sequence alignment of turkey β_1 AR and human adrenoreceptors around position 4.56 in TM4 showing the conserved proline at position 4.60.

(b) Schematic representation of the hydrogen bond network between TM4 and TM5 involving V172(4.56) in β_1 AR. The hydrogen bond network (orange dotted lines) originates at the carbonyl of V172(4.56) and connects to TM5 via two water molecules (w1 and w2, red asterisks).

(c, left) Phi and psi dihedral angles (averages and standard deviations in case of multiple chains) in TM4 between residues 4.48 and 4.61 for different complexes of β_1 AR (ligand, PDB code [chain]: carvedilol, 4AMJ [A,B]; cyanopindolol, 2VT4 [B,D] and 4BVN [A]; dobutamine, 2Y00 [A,B] and 2Y01 [A,B]; isoprenaline, 2Y03 [A,B]). V165(4.49) and V172(4.56), for which ^1H - ^{15}N resonances could be observed, are shown on a green and red background, respectively.

(c, right) Average of the ^1H - ^{15}N resonance positions for V165(4.49, green) and V172(4.56, red). The phi and psi values of V172(4.56) are distorted from the normal helical angles due to the loss of the intra-helical hydrogen bond to P176(4.60). Together with the loss of the canonical hydrogen bond, this strongly shifts both the ^1H and ^{15}N chemical shifts of V172(4.56) towards smaller ppm values relative to V165(4.49), which has normal, helical phi and psi angles.

(d) Partial views of the crystal structures of the carvedilol complex (PDB code 4AMJ), the isoprenaline complex (PDB code: 2Y03) and a docking model of the atenolol complex based on the cyanopindolol complex crystal structure (PDB code 4BVN). In the carvedilol complex, one water molecule (w2) forms a hydrogen bond network between the carbonyl oxygen of V172(4.56) and the side chains of S211(5.43) and S215(5.461). In the isoprenaline complex, the side chains of S211(5.43) and S215(5.461) are rotated and form hydrogen bonds to the catechol hydroxyl groups of isoprenaline. In this structure, no water molecule is observed at the equivalent position of w2. In the atenolol complex, the *para*-substituted acetamide of the ligand head ring (dashed circle) inserts between S211(5.43) and S215(5.461) and disturbs the

interface between TM3 and TM5 near V172(4.56) (solid circle).

Extended Data Figure 3: Response to various ligands for all assigned valine ^1H - ^{15}N resonances in TS- $\beta_1\text{AR}$. Color coding as in Extended Data Figure 1: cyan (atenolol), blue (isoprenaline), orange (dobutamine), purple (alprenolol), red (carvedilol), green (cyanopindolol), black (apo receptor). For clarity the centers of resonances are marked by circles. Firmly (tentatively) assigned residues are marked in black (cyan).

Extended Data Figure 4: Evidence for micro- to millisecond dynamics at the ligand entry/exit pathway. (Left) Region of the ^1H - ^{15}N TROSYs showing the V314(6.59) ^1H - ^{15}N resonance of TS- $\beta_1\text{AR}$ in the apo and various ligand-bound forms. The resonances of the apo and atenolol-bound forms are severely broadened in the ^{15}N dimension indicative of backbone dynamics in the micro- to millisecond range. The broadening is not observed for the other more tightly binding ligands. The resonances for the low affinity ligands, atenolol, isoprenaline and dobutamine, and for the high affinity ligands, alprenolol, carvedilol and cyanopindolol cluster at different positions. Interestingly, the resonance of the apo form clusters with the high affinity ligands, indicative of a similar backbone conformation. (Right) ^{15}N and ^1H line widths of the V314(6.59) resonance for the apo and ligand-bound forms of TS- $\beta_1\text{AR}$.

Extended Data Figure 5: Isoprenaline-induced activation of $\text{G}\alpha\text{i}\beta\text{1}\gamma\text{1}$ by $\beta_1\text{AR}$ mutants. G protein activation was measured by the change in tryptophan fluorescence upon exchange of GDP for $\text{GTP}\gamma\text{S}$ in the $\text{G}\alpha$ subunit of the heterotrimeric G protein. The figure shows the time courses of tryptophan fluorescence after the addition of different mutant forms of TS- $\beta_1\text{AR}$ in nanodiscs and $\text{GTP}\gamma\text{S}$ to the heterotrimeric G protein in the presence (red) and absence (black) of the agonist isoprenaline. The increase in fluorescence intensity at time $t = 0$ is caused by the additional fluorescence of the receptor, the nanodisc scaffold protein and the ligand. For the active mutant TS- $\beta_1\text{AR}_{\text{A227Y/L343Y}}$, this initial rise is followed by an exponential fluorescence increase due to the activation and dissociation of the G protein.

The rate of the $\text{G}\alpha\text{i}$ activation by TS- $\beta_1\text{AR}_{\text{A227Y/L343Y}}$ (half life ~ 290 s at 6 nM receptor) is approximately 4 times slower than for the activation by rhodopsin (half life ~ 400 s at 1 nM receptor) using the same assay. This assumes that the K_m of $\text{G}\alpha\text{i}$ for TS- $\beta_1\text{AR}_{\text{A227Y/L343Y}}$ is of the same scale as for rhodopsin (8.6 nM) and therefore significantly below the (saturating) concentration of $\text{G}\alpha\text{i}$ (100 nM). Each mutant was measured three times except for TS- $\beta_1\text{AR}_{\text{A227Y/L343Y}}$ that was measured four times. Representative fluorescence curves from single experiments are shown.

Extended Data Figure 6: Observed NMR effects of the reverse mutations of TS- $\beta_1\text{AR}$ towards the native $\beta_1\text{AR}$ sequence.

(a) ^1H - ^{15}N TROSY spectra of TS- $\beta_1\text{AR}$ and several reverse single and double mutants in complex with either atenolol (cyan) or isoprenaline (dark blue). Resonances are marked with assignment information (black: definite, cyan: tentative).

(b) Enlarged regions of the ^1H - ^{15}N correlation spectra showing only the resonance positions of V226(5.57) and V280(6.25) for all mutants in both ligand-receptor complexes. The black bar

represents 0.1 ppm in ^1H and 1 ppm in ^{15}N . For all mutants, the resonances for V226(5.57) show efficacy-related chemical shift changes between atenolol (diamonds) and isoprenaline (circles). For the A227Y mutants TS- $\beta_1\text{AR}_{\text{A227Y}}$ (green), TS- $\beta_1\text{AR}_{\text{V129I/A227Y}}$ (orange) and TS- $\beta_1\text{AR}_{\text{A227Y/L343Y}}$ (cyan), the ^1H - ^{15}N resonances of V226(5.57) also exhibit an overall shift due to a ring current effect from the introduced Y227(5.58) side chain, which has no structural significance. However, the V129I mutants TS- $\beta_1\text{AR}_{\text{V129I}}$ (red) and TS- $\beta_1\text{AR}_{\text{V129I/A227Y}}$ (orange) exhibit further ^1H - ^{15}N shifts towards a more active (i.e. bent) state of TM5 relative to the mutants that carry the V129(3.40) residue. For all mutants, the V280(6.25) resonances fall basically in identical positions and show no changes between atenolol and isoprenaline.

Extended Data Figure 7: Binding of NB80 to agonist-activated TS- $\beta_1\text{AR}_{\text{A227Y/L343Y}}$.

(a) Sequential addition of isoprenaline (1 mM, blue), NB80 (120 μM , red), and cyanopindolol (1 mM, green) to TS- $\beta_1\text{AR}_{\text{A227Y/L343Y}}$ (120 μM) followed by ^1H - ^{15}N TROSY spectra. Addition of an equimolar amount of NB80 changes the spectrum drastically. Except for few resonances (62, 89, 102, 103, 172, 280 and 326), the assignments are not transferable from the isoprenaline complex. The addition of cyanopindolol to this mixture apparently replaces isoprenaline in the receptor and drives the spectrum to the purely cyanopindolol-bound form. These results indicate that TS- $\beta_1\text{AR}_{\text{A227Y/L343Y}}$ can be activated, but that the fully active state requires stabilization with a G protein-like partner at the intracellular site.

(b) Changes in isoprenaline affinity of $\beta_1\text{AR}$ induced by NB80 binding. The isoprenaline affinity was assayed for TS- $\beta_1\text{AR}_{\text{A227Y/L343Y}}$ (green) and the truncated native turkey $\beta_1\text{AR}$ receptor (t β trunc, blue)¹⁷ by radio-ligand competition using ^3H -dihydroalprenolol in the presence of saturating amounts of NB80 (10 μM) or its absence. For TS- $\beta_1\text{AR}_{\text{A227Y/L343Y}}$ and t β trunc the apparent affinity increases by two log units in the presence of NB80, whereas no change occurs for TS- $\beta_1\text{AR}$. Data points are shown as mean and standard deviation of three independent experiments for each condition.

(c) Combined ^1H and ^{15}N chemical shift changes ($\Delta\delta = (\Delta\delta_{\text{1H}}^2/2 + \Delta\delta_{\text{15N}}^2/50)^{1/2}$) between the isoprenaline-TS- $\beta_1\text{AR}_{\text{A227Y/L343Y}}$ and the NB80-isoprenaline-TS- $\beta_1\text{AR}_{\text{A227Y/L343Y}}$ complexes as a function of residue number. Except for the few assigned peaks in the NB80-isoprenaline-TS- $\beta_1\text{AR}_{\text{A227Y/L343Y}}$ complex, chemical shift deviations are calculated as the minimal difference from the isoprenaline peak position to the nearest peak position in the isoprenaline-NB80 complex. Note that these minimal chemical shift deviations present a lower boundary for the deviations that could be obtained from a full assignment of the isoprenaline-NB80 complex. Peak deviations are color-coded in red (≥ 0.2 ppm), orange (0.2–0.05 ppm), blue (< 0.05 ppm), and grey (ambiguity from peak overlap).

(d) Representation of the chemical shift response to nanobody binding given in (c) on the structure of $\beta_1\text{AR}$. Valines in TM1 and TM7 do not show a large chemical shift response. Due to overlap the response for V280(6.25) in TM6 is unclear. Valines in TM2 show a strong response around the sodium binding region near residue D87(2.50), but valines at its extracellular side are not responsive. In general, valine resonances at the extracellular sides of TM3–6 are severely shifted. This indicates that the NB80 binding at the intracellular side has a long-range effect on the extracellular side, near the ligand binding site.

Extended Data Table 1: Pharmacological and geometrical properties of the β_1 AR ligands used in this study

	pharmacology				geometry	
	pK_D b36-m23*	pK_i TS- β_1 AR†	pIC_{50} TS- β_1 AR‡	Gs efficacy t β trunc§	insertion depth	tail volume¶
cyanopindolol	10.01 ± 0.11	>8.4 ± 0.3 [#]	>8.1 ± 0.1 [#]	39 ± 1	7.22	90.11
carvedilol	8.72 ± 0.09	>8.3 ± 0.3 [#]	>7.9 ± 0.1 [#]	12 ± 0.4	7.62	163.47
alprenolol	7.35 ± 0.07	7.6 ± 0.3	7.2 ± 0.1	31 ± 2	7.25	73.87
dobutamine	5.49 ± 0.03	5.0 ± 0.3	4.6 ± 0.1	112 ± 7	8.46	170.34
isoprenaline	5.16 ± 0.05	4.9 ± 0.3	4.6 ± 0.2	100	7.92	73.87
atenolol	4.29 ± 0.11	5.0 ± 0.3	4.6 ± 0.2	2.1 ± 1	ND [⊙]	73.87

* Values for binding affinity correspond to the β 36-m23 construct, which contains C- and N-terminal deletions and six thermostabilizing mutations¹⁰. The $pK_D = -\log K_D$ [M] was obtained from ³H-CGP12177 whole cell binding assays in stably expressed CHO cells¹⁷.

† pK_i values were obtained from the pIC_{50} values given in column 3 by adding $\log(1+[lig]/K_D) = 0.366$ as a correction for the concentration of the ³H-dihydroalprenolol (³H-DHA) ([lig] = 20 nM) and its determined dissociation constant ($K_D = 15.1 \pm 7$ nM, see Methods). Errors are obtained by error propagation from the errors of the pIC_{50} values and K_D .

‡ pIC_{50} values were determined by the radioligand inhibition assay described in the Methods section using ³H-DHA. Data are given as mean and standard deviation of three independent experiments.

§ Values for efficacy towards Gs-mediated signaling as determined by adenylyl cyclase activation of the truncated native turkey β_1 AR receptor (t β trunc)¹⁷. The efficacies are indicated as the percentage of the (maximal) isoprenaline response obtained from ³H-cAMP accumulation assays in CHO cells.

|| The insertion depth [Å] of the ligand was taken as the distance between the β -carbon atom of the ligand amino group and the amide nitrogen atom of V125 (V117 for β_2 AR) in the crystal structures of turkey β_1 AR in complexes with isoprenaline (PDB ID: 2Y03), dobutamine (PDB ID: 2Y00), carvedilol (PDB ID: 4AMJ), and cyanopindolol (PDB ID: 4BVN) as well as of human β_2 AR in complex with alprenolol (PDB ID: 3NYA).

¶ The tail volumes [Å³] were calculated by the Molinspiration Property Calculation Service (<http://www.molinspiration.com/cgi-bin/properties>) for the tail group including the amino moiety.

The pK_i and pIC_{50} are limited by the K_D and concentration of the radioactive tracer ligand as well as by the concentration of the receptor in the competition assay.

⊙ Not determined, no crystal structure available.

Extended Data Table 2: Sequence-specific assignment ^1H - ^{15}N valine resonances

Assigned residue	Position	Point mutation	Spectra with ligands	Further information
V62	1.53	V62A	Ate, Apo, Alp	
V90	2.53	V90A	Ate, Alp, Car, Cya	HN(CO)
V94	2.56	V94A	Alp, Car, Cya	
V102	2.54	V102A	Ate, Apo, Alp, Iso, Dob, Car, Cya	
V122	3.33	V122A	Alp, Car, Cya	
V125	3.36	V125A/I	Alp(A), Car(A), Ate(I), Apo(I)	
V129	3.40	V129I	Ate	
V134	3.45	V134A	Ate	
V160	4.44	V160A	Ate	
V172	4.56	V172A	Ate, Alp	Pred
V202	ECL	V202A	Alp	Pred
V226	5.57	V226A	Alp, Car, Cya	
V230	5.61	V230A	Alp	
V280	6.25	V280A	Alp, Car, Cya	
V298	6.43	V298A	Ate	HN(CO)
V314	6.59	V314A	Alp, Car, Cya	
V326	7.36	V326A	Alp	
V89	2.52	-	Ate, Apo, Alp, Iso, Dob, Car, Cya	HB, NM
V95	2.57	-	Ate, Apo, Alp, Iso, Dob, Car, Cya	HB, NM, HN(CO)
V103	2.65	-	Ate, Apo, Alp, Iso, Dob, Car, Cya	HB, NM, HN(CO)
V165	4.49	-	Ate, Apo, Alp, Iso, Dob, Car, Cya	NM

Ate: atenolol, Alp: alprenolol, Iso: isoprenaline, Dob: dobutamine, Car: carvedilol, Cya: cyanopindolol

HN(CO): information from 2D-filtered HN(CO) of ^{15}N , ^{13}C -Gly, Val, ^{15}N -Leu labeled receptor

Pred: ShiftX2 ^{15}N chemical shift prediction³¹

HB: expected $^1\text{H}^{\text{N}}$ shift based on hydrogen bond length analysis

NM: peak shift due to mutation of neighboring residue

Assignments for V89(2.52), V95(2.57), V103(2.65), V122(3.33), and V165(4.49) are tentative. V51(1.42), V52(1.43), V56(1.47), V60(1.51), V309(6.54), V312(6.57), and V320(ECL) have not been assigned.

Extended Data Table 3: Summary of the NMR response to ligands, G protein activation and NB80 binding data for the original TS- β_1 AR construct and various reverse mutants towards the native β_1 AR sequence

mutant name	residue			V226 response*	V280 response*	G protein activation†	NB80 binding‡	T _m [°C]§
	129	227	343					
original TS- β_1 AR	V	A	L	+	-	-	- (4.55/4.52)	58.9 +/- 0.6
TS- β_1 AR _{V129I}	I	A	L	+	-	-	N.D.¶	58.6 +/- 0.2
TS- β_1 AR _{A227Y}	V	Y	L	+	-	-	-	54.9 +/- 0.1
TS- β_1 AR _{L343Y}	V	A	Y	+	-	-	-	54.7 +/- 0.3
TS- β_1 AR _{V129II/A227Y}	I	Y	L	+	-	-	N.D.	54.4 +/- 0.1
TS- β_1 AR _{A227Y/L343Y}	V	Y	Y	+	-	+	+ (4.36/6.32)	47.8 +/- 0.2

* determined from the shifts of the ¹H-¹⁵N resonances in response to binding of atenolol and isoprenaline (see Extended Data Figure 6B).

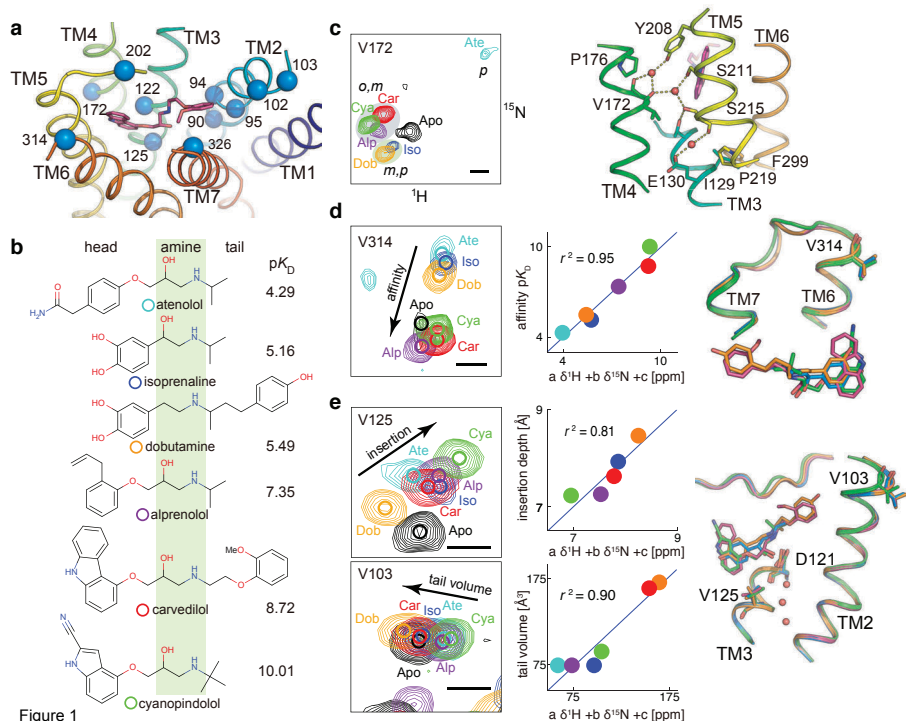
† determined from the G α i1 β 1 γ 1 activation assay described in Extended Data Figure 5.

‡ determined from NMR experiments by mixing of isoprenaline-activated TS- β_1 AR with NB80. The ¹H-¹⁵N spectra are shown for TS- β_1 AR_{A227Y/L343Y} in Extended Data Figure 7. The spectra of the other TS- β_1 AR mutants showed no response to addition of NB80 up to equimolar concentrations of ~100 μ M for both proteins. Values in parentheses show pIC₅₀ for isoprenaline binding in the absence or presence of NB80, respectively (see Extended Data Figure 7).

§ melting temperature T_m of the apo form receptor determined by the CPM thermal shift assay.

|| native residues are highlighted in bold.

¶ not determined.



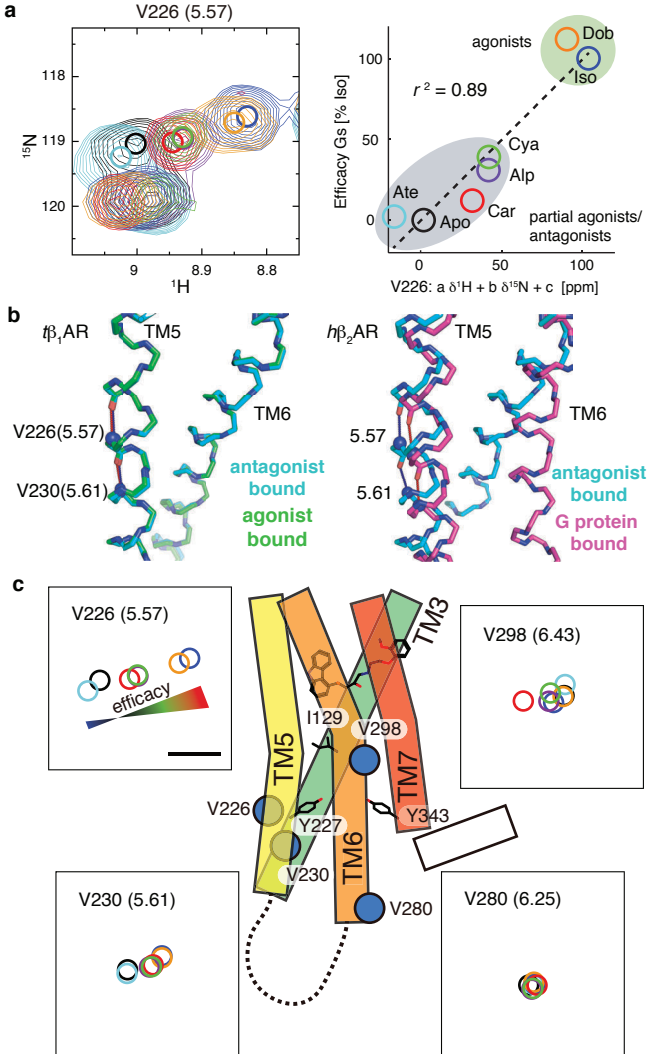


Figure 2

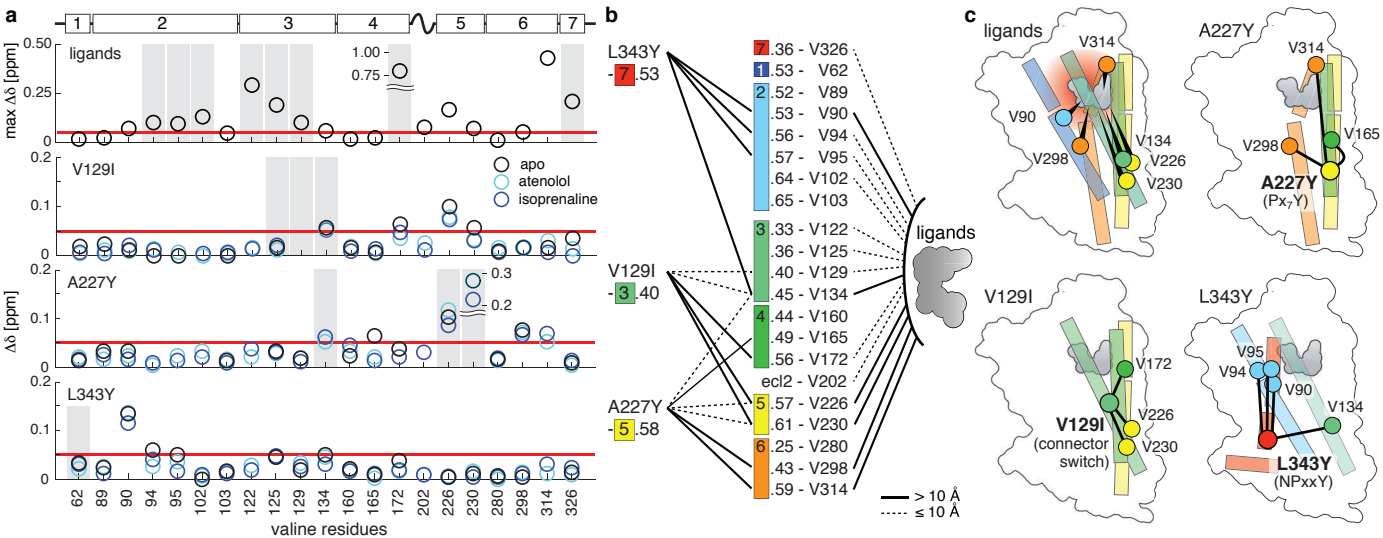
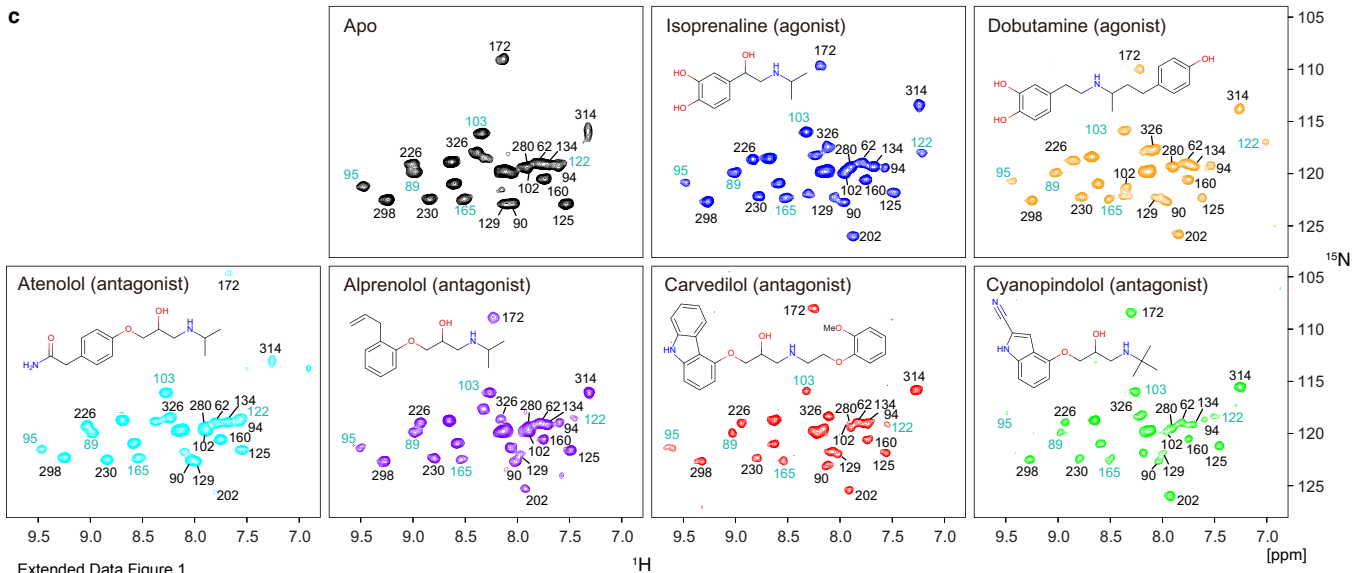
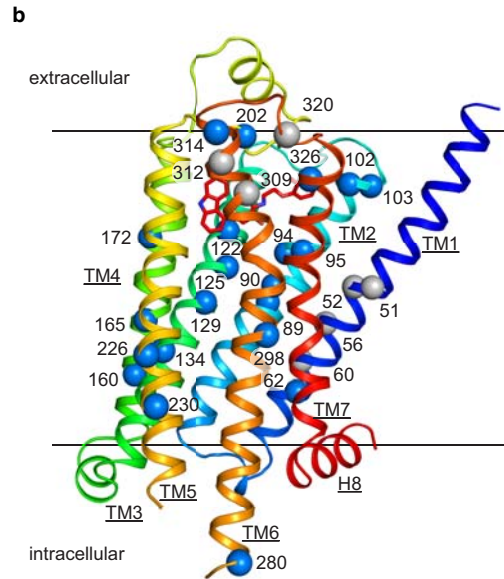
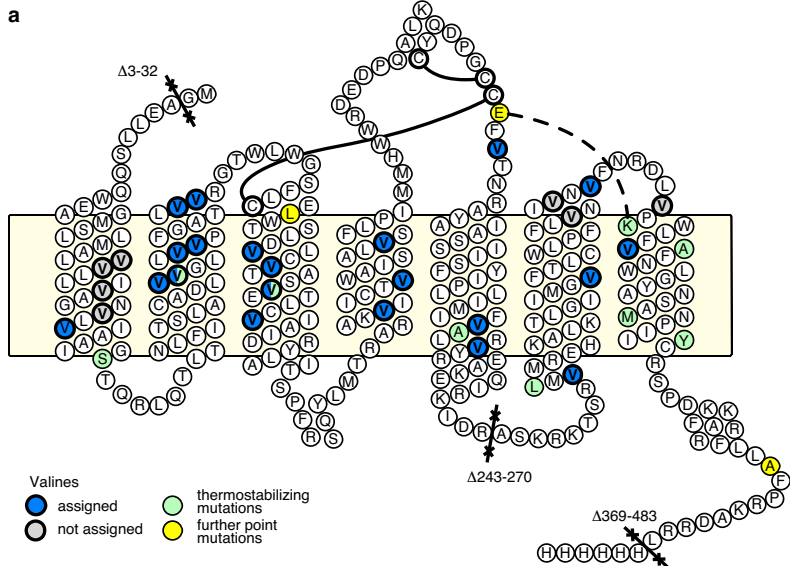
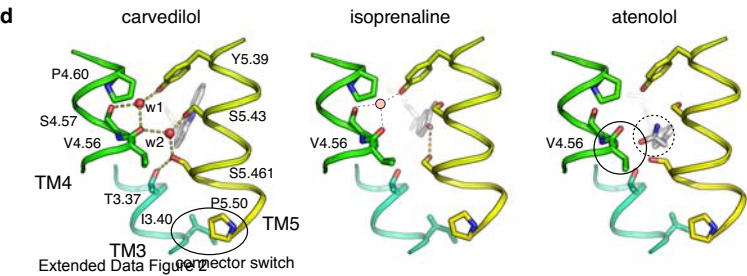
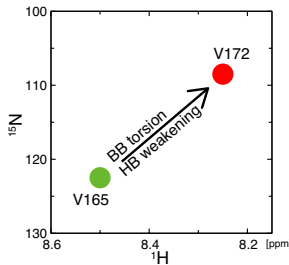
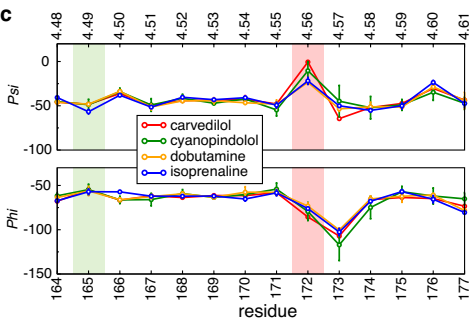
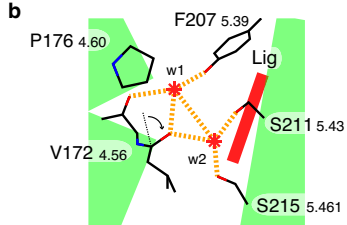
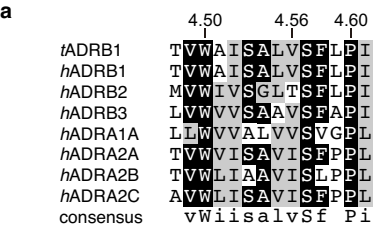
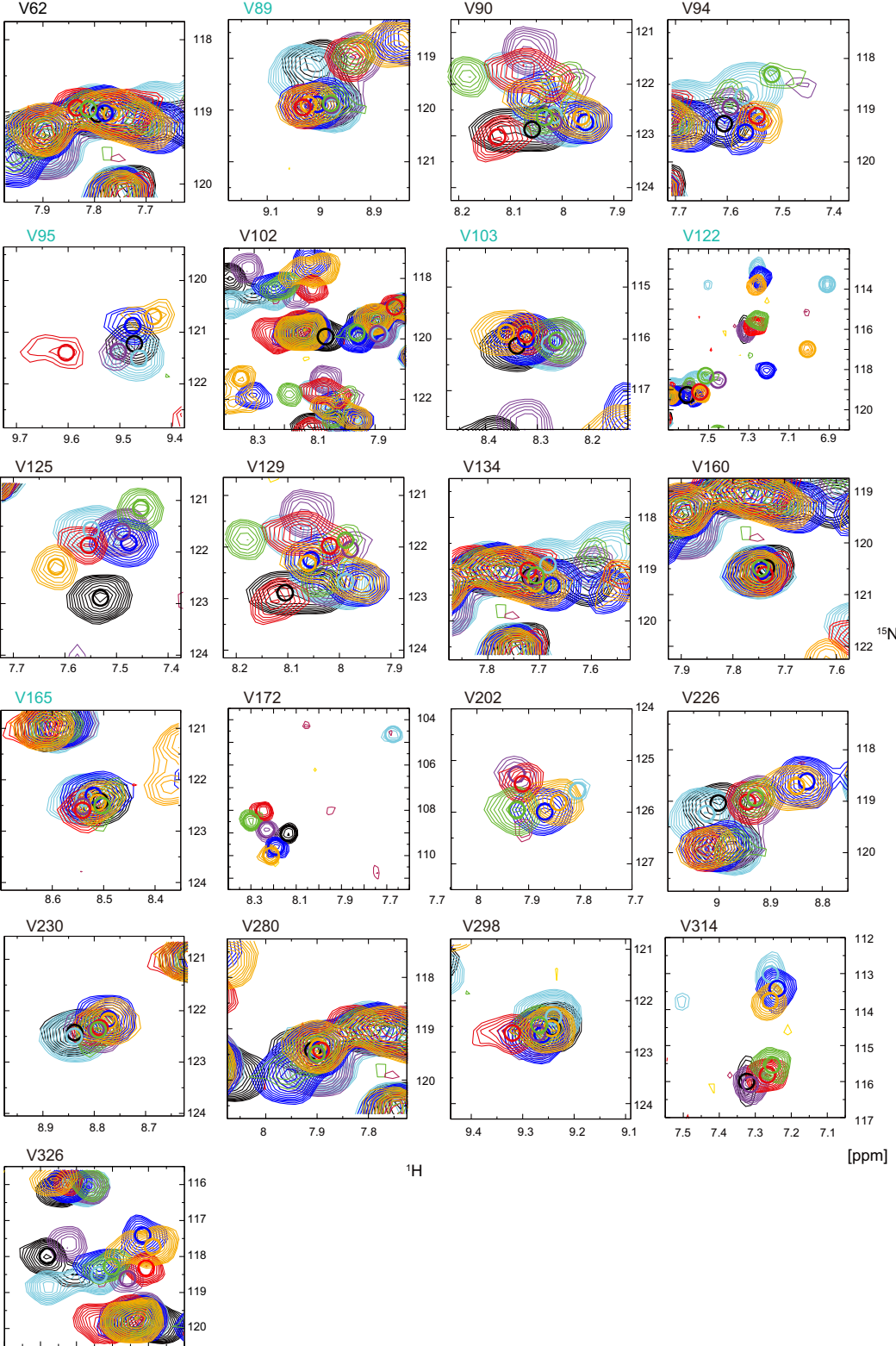
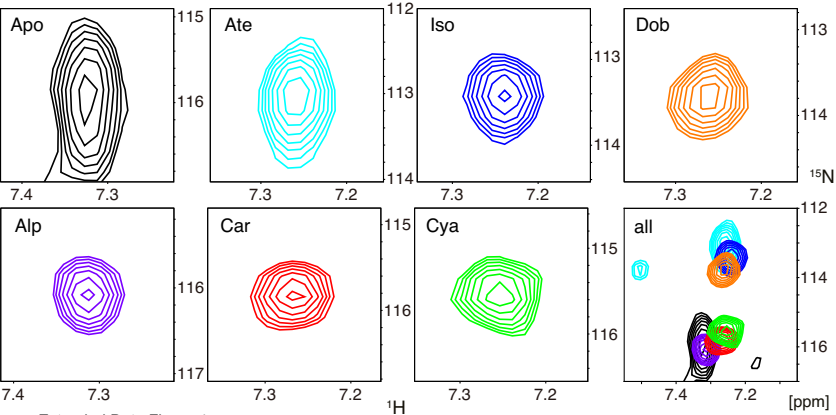


Figure 3



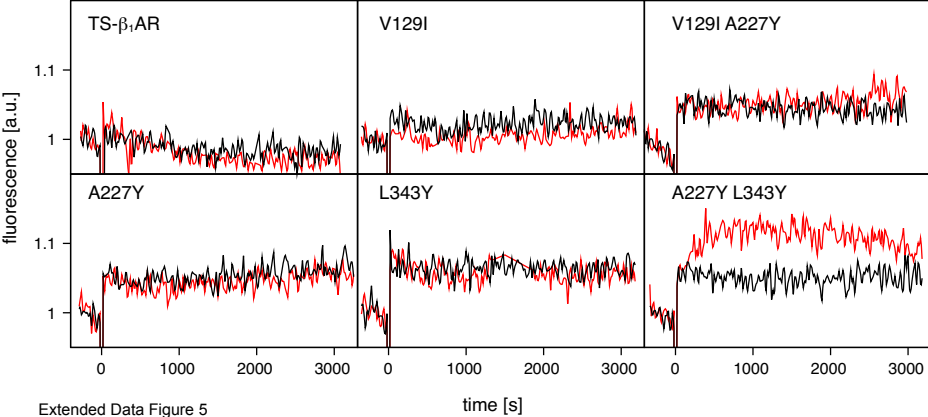




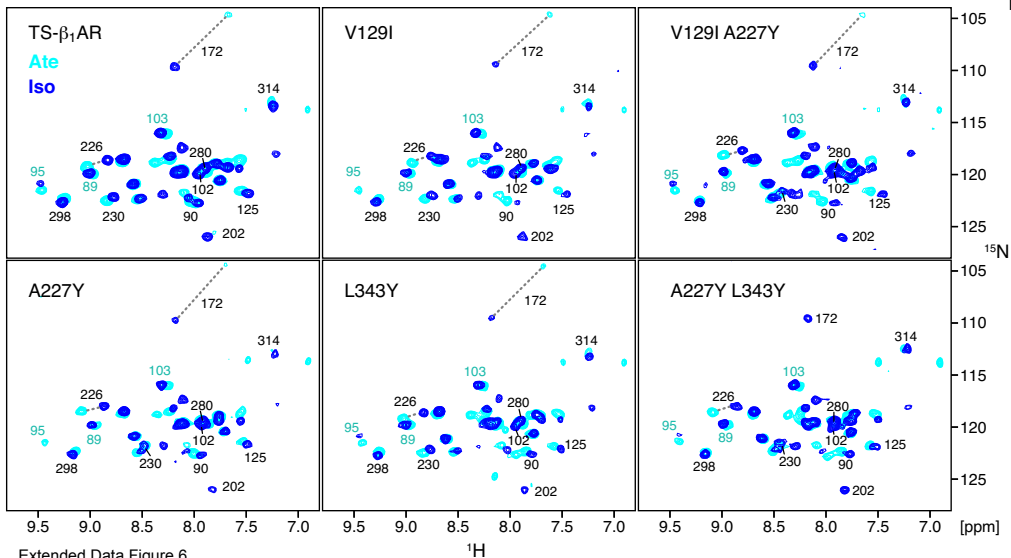


Ligand	Linewidth [Hz]	
	^{15}N	^1H
Apo	112.6	43.6
Ate	77.3	44.5
Iso	52.3	46.8
Dob	41.7	46.1
Alp	47.4	43.0
Car	40.0	50.4
Cya	37.7	48.1

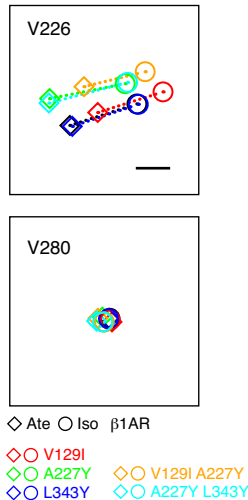
Extended Data Figure 4

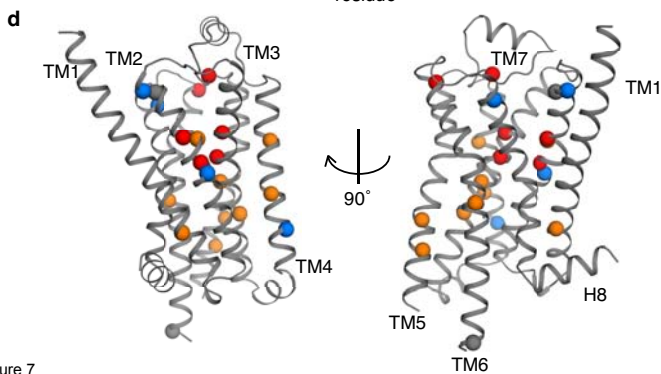
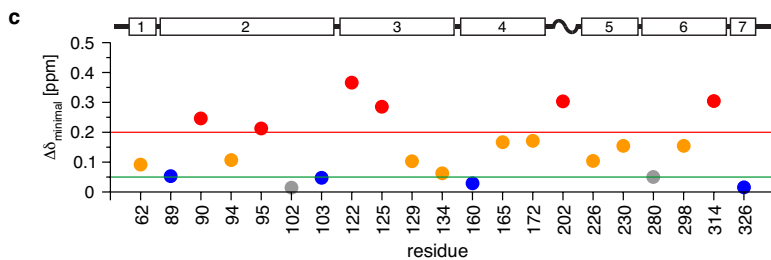
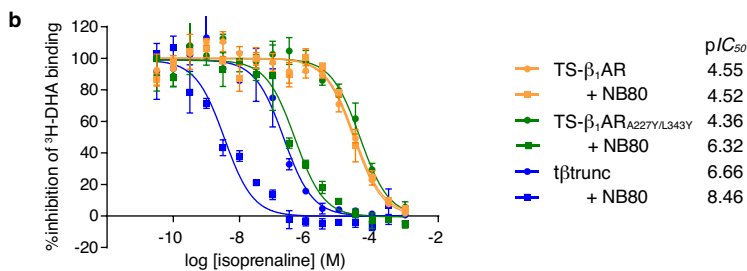
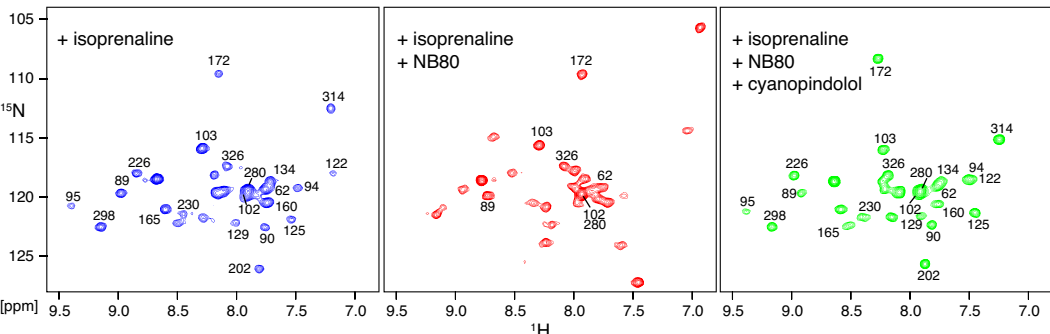


Extended Data Figure 5

a

Extended Data Figure 6

b



Backbone NMR reveals allosteric signaling networks in the β_1 -adrenergic receptor

Supplementary Information

Shin Isogai¹, Xavier Deupi², Christian Opitz¹, Franziska M. Heydenreich², Ching-Ju Tsai², Florian Brueckner², Gebhard F.X. Schertler^{2,3*}, Dmitry B. Veprintsev^{2,3*} and Stephan Grzesiek^{1,*}

¹ Focal Area Structural Biology and Biophysics, Biozentrum, University of Basel, CH-4056 Basel, Switzerland

² Paul Scherrer Institute, CH-5232 Villigen PSI, Switzerland

³ Department of Biology, ETH Zurich, CH-8093 Zurich, Switzerland

*corresponding authors

Stephan Grzesiek
Focal Area Structural Biology and Biophysics, Biozentrum
University of Basel, CH-4056 Basel, Switzerland
Phone: ++41 61 267 2100
FAX: ++41 61 267 2109
Email: Stephan.Grzesiek@unibas.ch

Dmitry B. Veprintsev
Paul Scherrer Institute, CH-5232 Villigen PSI, Switzerland
Email: dmitry.veprintsev@psi.ch

Gebhard F.X. Schertler
Paul Scherrer Institute, CH-5232 Villigen PSI, Switzerland
Email: gebhard.schertler@psi.ch

Text 1. Estimation of hydrogen bond length change from $^1\text{H}^N$ chemical shift change and uncertainty of crystal structure coordinates

The correlation between hydrogen bond length d_{HO} and amide proton chemical shift δH^N can be expressed as¹

$$\delta H^N = 19.2 \cdot \text{\AA}^3 \cdot d_{\text{HO}}^{-3} - 2.3$$

where δH^N is given in ppm and d_{HO} is the distance between amide hydrogen and carbonyl oxygen atoms. Taking the derivative relative to the distance d_{HO} yields

$$\frac{d\delta H^N}{dd_{\text{HO}}} = -3 \cdot 19.2 \cdot \text{\AA}^3 \cdot d_{\text{HO}}^{-4}$$

A finite small change Δd_{HO} in hydrogen bond distance can then be calculated from a finite small chemical shift change $\Delta \delta H^N$ as

$$\Delta d_{\text{HO}} \approx \frac{-d_{\text{HO}}^4}{3 \cdot 19.2 \cdot \text{\AA}^3} \Delta \delta H^N$$

Using $\Delta \delta H^N = -0.2$ for the change from the atenolol-bound to the isoprenaline-bound V226 resonances and $d_{\text{HO}} = 1.9 \text{ \AA}$ then yields a value $\Delta d_{\text{HO}} = 0.045 \text{ \AA}$.

The uncertainty of crystal structure coordinates can be estimated from the Cruickshank diffraction-component precision index (DPI)². For the currently highest resolution GPCR structure (human δ opioid receptor³, 1.80 \AA resolution), the DPI is 0.127 \AA , which is larger than the small H-bond distance change detected by NMR.

References

1. Grzesiek, S., Cordier, F., Jaravine, V. & Barfield, M. Insights into biomolecular hydrogen bonds from hydrogen bond scalar couplings. *Prog Nucl Mag Res Sp* **45**, 275–300 (2004).
2. Cruickshank, D. W. J. Remarks about protein structure precision. *Acta Crystallogr D Biol Crystallogr* **55**, 583–601 (1999).
3. Fenalti, G. *et al.* Molecular control of δ -opioid receptor signalling. *Nature* **506**, 191–196 (2014).